Optimal Design of a Novel High-Power Thyristor-based DC Circuit Breaker

Siavash Beheshtaein, Mandana Saravani, Farzad Banihashemi, and Robert Cuzner
University of Wisconsin Milwaukee, Milwaukee, USA
beheshta@uwm.edu, sheikhz2@uwm.edu, banihas2@uwm.edu, cuzner@uwm.edu

Abstract— **Due to dc microgrid nature, dc fault current has no zero-crossing current and could increase up to a thousand amps. Because of that, a dc circuit breaker (DCCB) with the ultra-fast response and high efficiency is required. Regarding this issue, this paper presents a novel thyristor-based DCCB. Then the optimal values of the proposed DCCB components are obtained by cost-power loss multi-objective optimization method. Finally, to keep the maximum temperature of the thyristor below the maximum allowed value, an optimum forced-air microchannel that has high reliability, low cost, and high efficiency is proposed for the proposed thyristor-based DCCB.**

Index Terms*— *dc circuit breaker, dc microgrid, fault, protection, Thyristor

I. INTRODUCTION

DC microgrids have attracted significant attention over the last decade in both academia and industry. Among many existing challenges, dc protection is considered as one of the main critical challenges to be addressed in order to facilitate the realization of a reliable and secure dc microgrid [1]. Due to high peak amplitudes on sudden short circuit fault inception, and no zero-crossing design of a dc circuit breaker (DCCB) with a sufficiently fast time response is critical. DCCBs fall under two categories, or types: Solid-state circuit breaker (SSCB) and Hybrid CB (HCB). The main advantage of the SSCB is the fast time response. However, because of potential high power loss, the resultant cooling system may significant in size and cost. The selection and configuration of the associated current limiting power semiconductors for low loss is also of paramount importance. One the other hand, the HCB has low power loss, but the operation time is still in the range of milliseconds.

The SSCB (see Fig. 1(a)) uses different solid-state power semiconductor devices, including the MOSFET, IGBT, IGCT, and thyristor. Among them, MOSFET has the lowest nominal voltage, as a result, is not practical for consideration in medium and high voltage applications. Recently, the Silicon Carbide MOSFET has emerged as a viable device for SSCB consideration, having an off-state voltage rating comparable to thyristors (up to 10kV). On the other hand, among the rest of the semiconductor device, thyristors have the lowest conduction losses (see Fig.1 (b)). Such a low on-state loss of thyristor switch results in the reduction of overall life-cycle costs of the SSCB and decreased investment in the cooling system of thyristor-based SSCBs. Furthermore, thyristor has a higher nominal voltage and current. Therefore, it is an appropriate candidate for medium/high voltage applications. However, the main drawback of thyristors is not able to turn off the current actively [3].

For medium voltage applications, the thyristor-based SSCB is a good candidate from current handling, loss, and cost standpoint, however, because of no zero-crossing in fault current, another device or circuit must be used in series with the thyristor in order to force the current to the zero. This paper proposed a new thyristor-based SSCB that uses a Current Commutation Drive Circuit (CCDC) that forces current to the zero during in order to isolate short circuit faults from a Medium Voltage DC (MVDC) system. With this implementation, there is no need to add a snubber or clamp circuit across the thyristor because the CCDC drives inductive current to zero before the thyristor commutates off. This feature also enhances the scale-ability of the DCCB with current because packaged implementations of a lower-rated DCCB building block can be connected in parallel without impact to the thyristor turn-off commutation stresses. Other advantages of the proposed DCCB are fast-time response, low cost, low power loss, voltage scalability, current scalability, and cooling system size. To achieve an optimal design of the proposed method, the magnetic part of the CCDC is implemented in ANSYS-MAXWELL software, and the optimum value of the CCDC is obtained based on cost-power loss multi-objective optimization technique. Finally, an advanced double-side forced air-cooling system, which was inspired by the internal cooling channels known as serpentine passages in the gas turbine blades, is proposed and build in STAR-CCM+ software to keep the surface temperature of thyristor below its limit. This cooling system approach is compact, lightweight, and has high reliability.

II. PROPOSED METHOD

In order to have an SSCB with low power loss, low cost, compact cooling system, and fast operation time, a new thyristor-based DCCB is designed. As shown in Fig. 1(c), the proposed DCCB is composed of a thyristor in series with a CCDC block. The CCDC block is designed based on a coupled inductor that the primary inductor is in series

978-1-7281-5826-6/20/$31.00 ©2020 IEEE

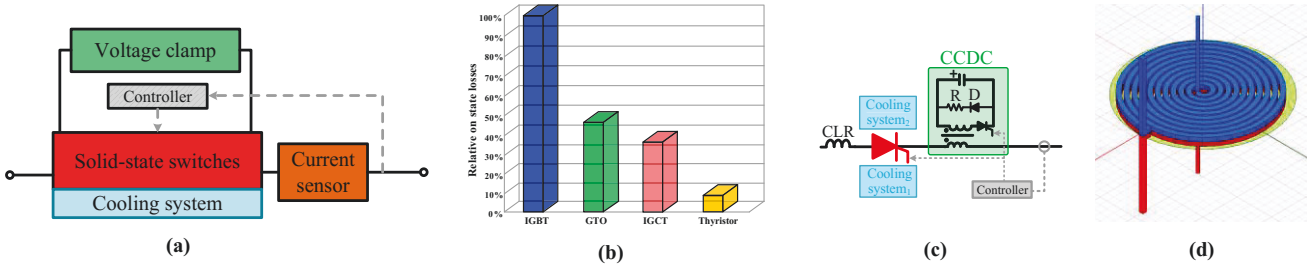

Fig. 1. DCCB: (a) A typical DCCB, (b) Relative on-state losses, (c) Proposed thyristor-based DCCB. (d) Coupled inductor ANSYS-Maxwell.

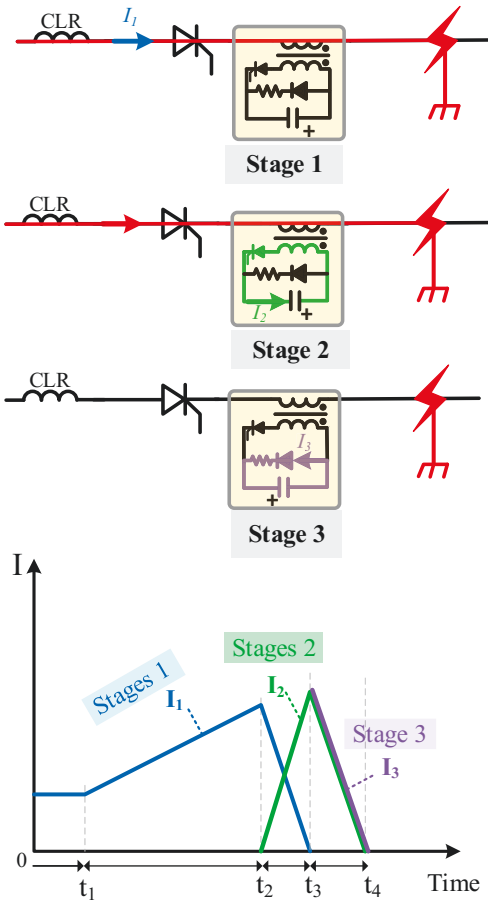

Fig. 2. Fault current stage in the proposed thyristor-based DCCB.

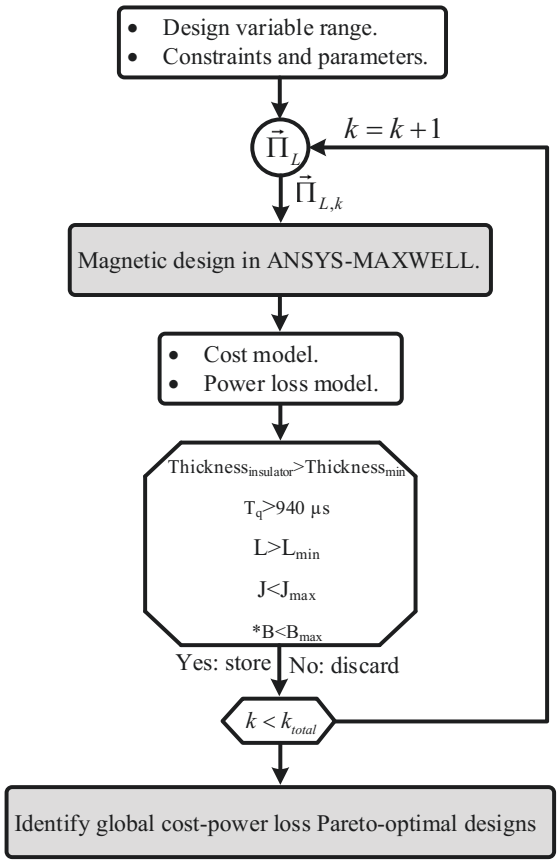

Fig. 3. Flowchart of the multi-objective optimization scheme.

with the thyristor, and the secondary inductor is connected to a pre-charged capacitor and thyristor. In addition, a resistor- diode (RD) branch is used in parallel with a capacitor for the dissipation capacitor current, when needed.

As shown in Fig. 2, the thyristor-based DCCB interrupts DC fault current in three stages. In the first stage, the fault current passing through the thyristor and primary side of the coupled inductor increases with respect to the fault impedance. Then, after the fault current exceeds a specific threshold, the fault is detected, the thyristor in the coupled inductor is closed and the capacitor can discharge its voltage. Because of negative mutual inductance, back EMF is generated in the primary side of the coupled inductor, which forces the fault current to zero.

Finally, after the capacitor current reaches a maximum value, the voltage polarity changes from positive to negative; in this situation, the RD branch dissipates the capacitor current. All these three operation stages are shown in Fig. 2. The CCDC of the DCCB highly affects the cost and power loss. In order to optimize cost versus losses, a multi-objective optimization process, outlined in Fig. Three is used to find suitable values for the CCDC shown in Fig. 2. According to Fig.3, design space variables of the coupled inductor primary number of turns (*Turn1*), coupled inductor secondary number of turn (*Turn2*), primary copper bar radius (R_{cs1}), secondary copper bar radius (R_{cs2}), the inner radius of the coupled inductor (R_{in}), and distance between primary and secondary coupled inductors (d) are taken into account. Since the DCCB is designed for a system having a nominal voltage and

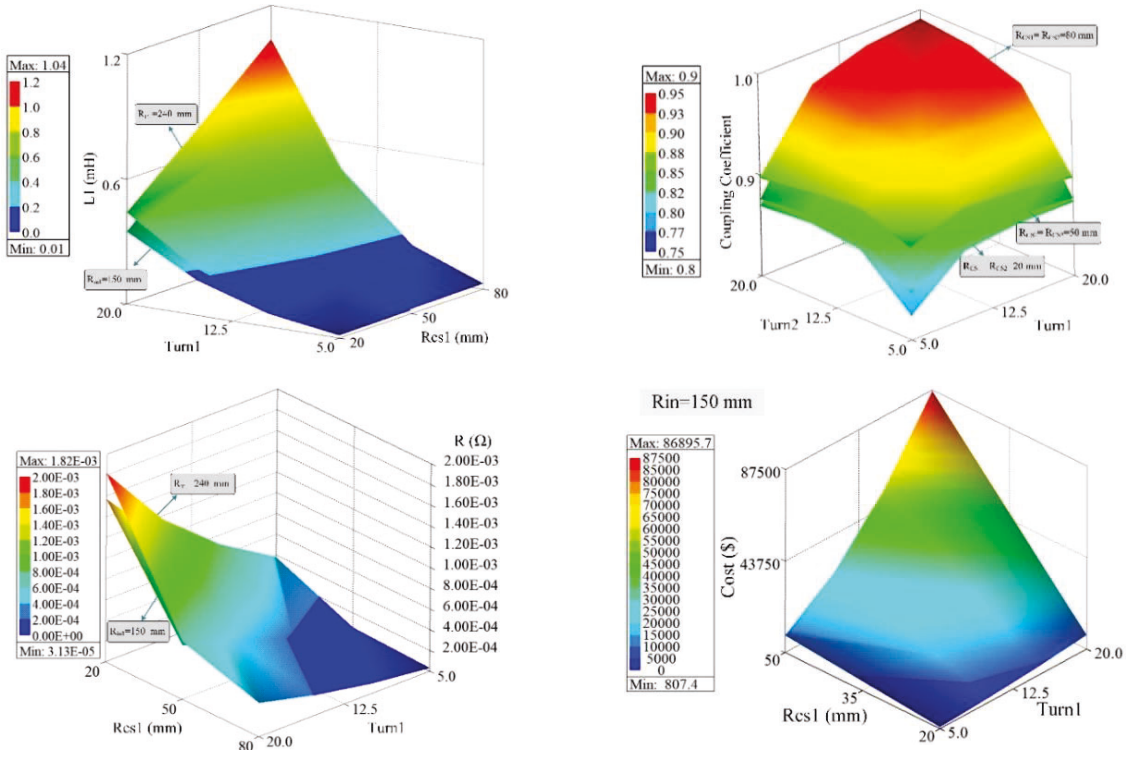

Fig. 4. ANSYS-Maxwell simulation results of the primary inductor, coupling coefficient, power loss, and coupled inductor cost.

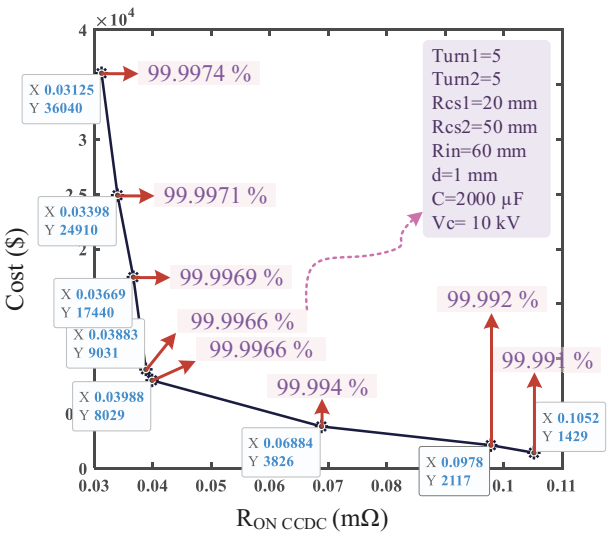

Fig. 5. Cost- power loss Pareto front.

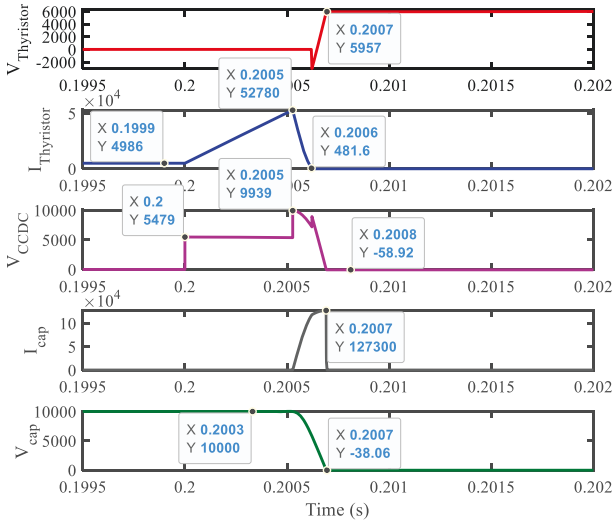

Fig. 6. Simulation results of the proposed method with parameters resulting in 99.9966% efficiency.

current are 6000 V, and 5000 A, the disk insulator of epoxy with the thickness of (V_{max}/ high dielectric strength =1mm) is considered [4]. On the other hand, with an increase in *d,* the coupling coefficient will be decreased. Therefore, it is assumed two inductors are attached to the epoxy. Then, the CCDC with each variable is implemented in ANSYS-Maxwell software (see Fig. 1(d)). In the third stage, power loss, as well as the cost of each topology is calculated. The cost of the CCDC is a function of capacitor and inductor costs, including epoxy that is obtained as follows:

$$\mathrm{Cost}_L = \overbrace{5*\omega_{epoxy}}^{\mathrm{Cost}_{core}} + \overbrace{6*\omega_{L1+L2}+1}^{\mathrm{Cost}_{L1+L2}} + \overbrace{7*\omega_{L1+L2}+1}^{\mathrm{Cost}_{Lab,L}} \quad (1)$$

$$\mathrm{Cost}_{cap} = -1.022\ \$ + 54.956*10^{-3}*U_{cap}\frac{\$}{V} + 2.426*10^{-3}*C_{cap}\frac{\$}{\mu F} \quad (2)$$

In the fourth stage, different constraints including minimum time required to keep thyristor (5STP52U5200) current to zero (T_q) that is equal to 940 µs, minimum

TABLE I. THYRISTOR SPECIFICATION.

Thyristor voltage threshold	1.05 V
On-state resistance	0.115 mΩ
Maximum controllable turn-off current	5000 A
Junction operation temperature	125 ˚C
Junction area	9503.32 mm^2
Thermal resistance junction-to-case (double side cooled),	8.5 K/kW
Thermal resistance case-to-heatsink (double side cooled)	3 K/kW
Calculated on-state power loss in each thyristor	3.35 kW

TABLE II. DIMENSIONS OF THE CHANNEL WITH 45˚ PARALLEL RIB.

Description	**Value**
Hydraulic Diameter (D_h)	24 mm
Rib Height to Channel Hydraulic Diameter Ratio (e/D_h)	0.132
Rib Pitch to Rib height Ratio (p/e)	10

primary inductor current to limit thyristor transient current, maximum current to zero (T_q) that is equal to 940 μs, minimum primary inductor current to limit thyristor transient current, maximum current density, and maximum flux density are applied. T_q can be calculated by the following state-state equation:

$$\begin{bmatrix} V_{dc\_grid} \\ V_c \end{bmatrix} = \begin{bmatrix} L_1 & M \\ M & L_2 \end{bmatrix} \begin{bmatrix} \dot{I}_1 \\ \dot{I}_2 \end{bmatrix} \tag{3}$$

$$V_c = V_{c0} - \frac{1}{c}\int I_2 dt$$

Regarding these considerations, *inductor1*, coupling coefficient, power loss, and cost that are obtained from modeling in ANSYS-MAXWELL are shown in Fig. 4. As shown in Fig. 4, the power loss as well as cost highly depends on R_{cs1}, *Turn1*, and R_{in}, therefore solving a multiobjective problem for designing the proposed DCCB is a must. As shown in Fig. 3, for each design, cost, and power loss objective functions are calculated, then the cost-power loss Pareto optimal design is obtained (Fig. 5). Therefore, according to the system requirement and budget, each of the system parameters could be selected from the Pareto front. For example, Fig. 6. shows the results for the CCDC parameters leading to 99.9966% efficiency.

III. COOLING SYSTEM DESIGN

For this study, a cooling system inspired by gas turbines cooling technology was designed. This cooling system helps to maintain the maximum junction temperature below the maximum allowance temperature. Table I describes the thyristor specification considered for this design.

In this paper, a four-passage channel with 180-deg turn was proposed. Additionally, 45-deg parallel rib turbulators were installed on the bottom and top walls of all passages to create more turbulence and increase the thermal efficiency of the cooling system. Each rib turbulator had a parallelogram cross-section of 6.35 × 6.35mm.

Fig. 7 describes the schematic of the cooling system. Also, Table II indicates the detailed dimensions of the

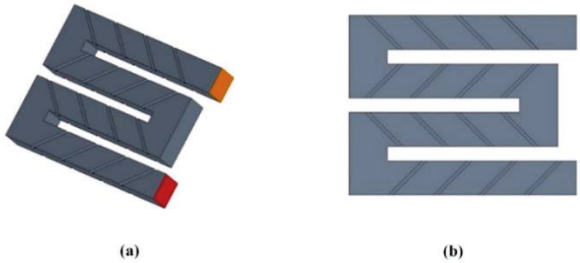

Fig. 7. Channel configuration (a) entire view, (b) Top view.

the geometrical model used in this study. As flow passes through these channels, a significant amount of heat is removed from the surface due to the forced convection heat transfer, which resulted in a noticeable decrease in the joint surface temperature.

A computational model of the proposed channel was developed. Computational Fluid Dynamic (CFD) analysis was carried out for temperature distribution and flow behavior inside the channel for various operating conditions. One of the primary design considerations in the cooling channel system design is to enhance the heat transfer coefficient while decreasing the pressure drop.

Pressure drop effects can be found in the friction factor relationship, as shown in (4) [5], where D_h is channel hydraulic diameter, L is the distance that the pressure is measured and ΔP is the pressure difference in the inlet and outlet of the channel. To normalize the friction factor Blasius relationship, which is the friction factor in a smooth circular tube, is used [5]. Furthermore, thermal performance can be calculated based on the Nusselt number enhancements and normalized friction factor. Thermal performance of the system can be calculated as:

$$f = \left(\frac{D_h}{2L}\right)\left(\frac{\Delta P}{\rho V_m^2}\right) \tag{4}$$

$$f_0 = 0.079\,\mathrm{Re}\,e^{(-0.25)} \tag{5}$$

$$\mathrm{Re} = \frac{\rho U D_h}{\mu} \tag{6}$$

$$\eta = \frac{(Nu/N_0)}{(f/f_0)^{1/3}} \tag{7}$$

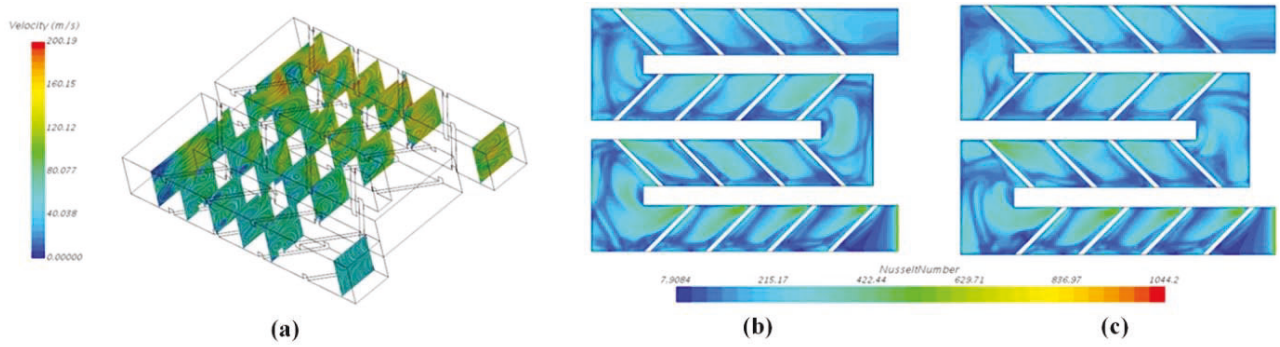

Fig. 8. (a) Vector velocity distribution along the channel on the normal planes Re=76000, (b) Local time average Nusselt number distribution for Re=76000 (top), (c) (bottom).

IV. Numerical Setup

Heat transfer inside the channel was analyzed by utilizing Star CCM+ commercial CFD package. Air as cooling fluid entered the channel at the ambient temperature and pressure condition (~300K and 100 kPa) with a uniform velocity normal to the inlet plane. Reynolds number for the inlet air passes the first passage was between 45000 to 90000. In this design, the top and bottom walls are considered to be installed between across thyristor. Thus, the power loss of each thyristor can be measured as the amount of rated heat power. In the presented work, 1700 W applied as a constant heat flux to the top and bottom wall, and rib turbulators, while other walls considered having an adiabatic boundary condition.

The Reynolds Average Navier-Stokes (RANS) model of k-ω along with the shear stress transport (SST) formulation is employed for modeling the implicit unsteady turbulent flow in the duct. For this study, each simulation ran for one second physical time. The time step size was 2.8E-4 seconds based on the CFL number of 0.9 and second-order accuracy. Also, the computational domain consists of around 10 million mesh elements along with ten prism layers near the solid walls. The average y^+ value was kept below 0.5 to ensure the proper boundary layer resolution for the turbulence model considered.

V. Thermal Cooling Results

Fig. 8(a) shows the vector velocity distribution along the channel for flow with a Reynolds number of 76000. As flow passed through the first passage, the velocity increased, which increased the turbulent. Increasing the velocity enhanced the mixing heat with the coolant flow, which increased the heat transfer ratio between coolant and channel walls. Fig. 8 (b) and (c) shows the time-averaged Nusselt number distribution along the channel on the top and bottom walls. As can be seen, after flow passed through each rib, the Nusselt number increased in all passages. In the turning regions, more turbulence was generated, which increased the Nusselt number in these regions. From the initial results, it can be observed the proposed design can enhance the heat transfer coefficient, which resulted in removing more heat from the thyristor surface in a small time frame. Results from the study of various rib turbulators and inlet Reynolds effect show that increasing the Reynolds number in a channel wit 45-deg rib increases the thermal performance by up to 85%.

VI. Conclusion and Future Works

High-power SSCB has high power loss that could lead to High-power SSCB has high power loss that could lead to both high power loss and big and expensive cooling systems. To deal with this issue, a new CCDC based thyristor DCCB, which has a low power loss, low cost, no need for snubber, and building block capability, is proposed. To make the proposed DCCB more efficient and cost-efficient. The CCDC part is modeled and optimized in ANSYS-Maxwell as well as in Matlab, respectively. Then, based on multi-objective optimization, a set of optimum results is obtained based Pareto front curve. As it is shown in the results, the proposed DCCB has efficiency from 99.991% to 99.9976%, and time response of fewer than 600 µs. In addition, regarding the specification of the thyristor, the required cooling system is in the range of the forced-air cooling system. Therefore, based on the calculated power loss and other specifications of thyristor, a new topology of air-forced microchannel cooling system inspired by the cooling system used for gas turbines is designed. According to the results, the proposed cooling system has a high transfer coefficient. This value could also be increased by considering other parameters such as the number and shape of ribs. The future work will be adding volume (weight) as another objective function and integrating of a jet impingement cooling into this design to increase the performance of the cooling system considerably.

References

[1] T. Dragicevic, L. Xiaonan, J. C. Vasquez, and J. M. Guerrero, "DC Microgrids — Part II : A Review of Power Architectures , Applications , and," *IEEE trans. Power Elecron.*, vol. 31, no. 5, pp. 3528–3549, 2016.

[2] S. Beheshtaein, M. Savaghebi, J. C. Vasquez, and J. M. Guerrero, "Protection of AC and DC Microgrids : Challenges , Solutions and Future Trends," in *Proc. 41th Annu. Conf. IEEE Ind. Electron. Soc. (IECON)*, 2015, pp. 5253–5260.

[3] S. Beheshtaein, S. Member, R. M. Cuzner, and S. Member, "DC Microgrid Protection : A Comprehensive Review," *IEEE J. Emerg. Sel. Top. Power Electron.*, vol. PP, no. c, p. 1, 2019.

[4] Z. Wang and G. Chen, "Study on Planar Busbar Regarding Stray Inductance Minimization and Oscillation Suppression for High Power Converter," in *2009 International Conference on Sustainable Power Generation and Supply*, 2009, pp. 1–7.

[5] Y. Liu, L. M. Wright, W. Fu, and J. Han, "Rib Spacing Effect on Heat Transfer and Pressure Loss in a Rotating Two-Pass Rectangular Channel (AR=1:2) with 45-Degree Angled Ribs," in *ASME Turbo Expo 2006: Power for Land, Sea and Air*, 2006, pp. 1–11.